

Polyamide Nanofiltration Membranes from Emulsion-mediated Interfacial Polymerization

Yuanzhe Liang ^{1,2,3}, Xiangxiu Teng¹, Rui Chen², Yuzhang Zhu^{1*}, Jian Jin^{1,4*}, Shihong Lin ^{2,3*}

Revised Manuscript Submitted to

ACS ES&T Engineering

¹ i-Lab and CAS Center for Excellence in Nanoscience, Suzhou Institute of Nano-Tech and Nano-Bionics, Chinese Academy of Sciences, Suzhou 215123, P.R. China

² Department of Civil and Environmental Engineering, Vanderbilt University, Nashville, TN 37235-1831, USA

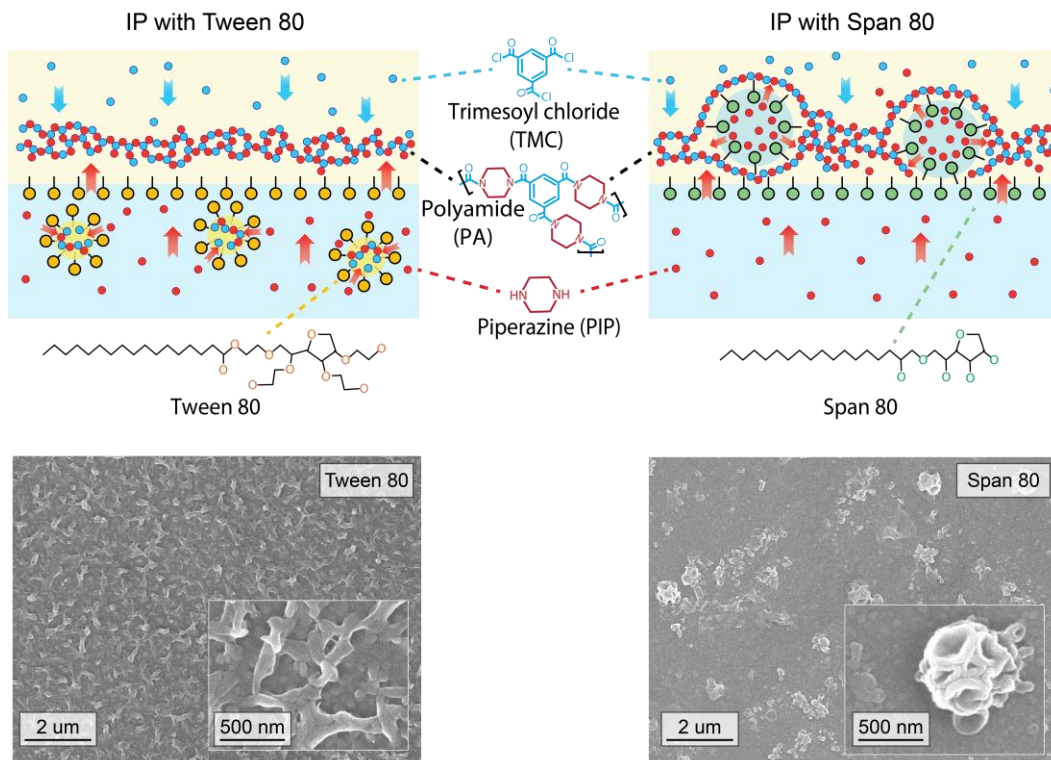
³ Interdisciplinary Material Science Program, Vanderbilt University, Nashville, TN 37235, USA

⁴ College of Chemistry, Chemical Engineering and Materials Science, Soochow University, Suzhou 215123, P. R. China

*Corresponding author email: yzzhu2011@sinano.ac.cn (Y. Zhu); jjin2009@sinano.ac.cn (J. Jin); shihong.lin@vanderbilt.edu (S. Lin)

TOC Art

Polyamide formation in interfacial polymerization with Tween 80 vs. Span 80



1 ABSTRACT

2 Fabrication of nanofiltration (NF) membranes using interfacial polymerization (IP) continues to
3 receive tremendous interest in research and development due to the broad applications of NF in
4 water treatment, wastewater reuse, and industrial separations. Many approaches have been
5 explored to enhance the performance of NF membranes by regulating the IP process. Among these
6 approaches, the use of surfactants has shown strong potential due to its low cost and compatibility
7 with existing infrastructure for membrane fabrication. While the different roles of the surfactants
8 have been increasingly elucidated in recent years, little is known for the role of emulsion formation
9 in the IP process. In this study, we investigate the impacts of nonionic, emulsifying surfactants on
10 the formation, properties, and performance of the polyamide NF membranes. Two surfactants were
11 compared, including the hydrophilic Tween 80, which is an oil-in-water (o/w) emulsifier added in
12 an aqueous solution of piperazine, and the lipophilic Span 80, which is a water-in-oil (w/o)
13 emulsifier added in the hexane solution of trimesoyl chloride. Our results illustrate the effects of
14 emulsions as “vehicles” to facilitate monomer transfer and as “microreactors” for providing
15 additional and distributed interfaces for IP. Depending on whether the surfactants are o/w or w/o
16 emulsifiers, the resulting membranes have unique physicochemical properties and NF
17 performance. In both cases, the addition of nonionic surfactants at low-to-moderate concentrations
18 results in smaller pore sizes and a narrower pore size distribution. Overall, this study provides
19 important insights into how the IP process and the resulting NF membranes are influenced by the
20 formation of emulsions.

21 **Keyword:** Interfacial polymerization, Emulsion, Nonionic surfactant, Thin-film-composite
22 polyamide membrane, Nanofiltration

23 **INTRODUCTION**

24 Growing water scarcity is one of the leading challenges of our time, impacting over one-third of
25 the world's population^{1,2}. To address this challenge, research has been actively performed to
26 explore more effective ways of tapping into unconventional sources to augment drinking water
27 supply and/or reusing wastewater to reduce water demand²⁻⁵. Among the various technical
28 approaches, membrane-based water and wastewater treatment technologies have received
29 tremendous interest due to their small footprint, high energy efficiency, modularity, and the
30 capability of achieving molecular separation^{2,6-8}. Specifically, nanofiltration (NF) is a low-
31 pressure membrane-based process that is widely used in brackish water desalination and
32 wastewater reclamation^{9,10}. Compared to reverse osmosis (RO) membranes used widely for
33 seawater desalination, NF membrane typically has a relatively 'loose' active layer that enables
34 operation at a lower pressure and/or a higher flux¹¹. More importantly, NF can also be employed
35 for selective separation of solutes from a mixed solution based on the various solute exclusion
36 mechanisms^{12,13}.

37 Most commercial NF (and RO) membranes are thin-film-composite (TFC) polyamide
38 membranes formed via a process called interfacial polymerization (IP)^{14,15}. In an IP process for
39 making NF membranes, a hexane solution of trimethylol chloride (TMC) is brought into contact
40 with porous support (typically an ultrafiltration membrane) pre-wetted with an aqueous solution
41 of piperazine (PIP). The PIP molecules diffuse across the water-hexane interface and react with
42 the TMC in the hexane phase to form a thin polyamide (PA) layer that serves as the active
43 separation layer¹⁶. While there exist other methods for fabricating NF/RO membranes, the IP
44 process is the most widely used in the industry because of its high manufacturing efficiency and
45 the robust separation performance of the resulting TFC-PA membrane^{9,17-19}.

46 Conventional IP fails to provide effective control of the membrane pore structure (e.g., pore
47 size and thickness) due to uncontrolled trans-interface diffusion of PIP monomers and the fast
48 polymerization between PIP and TMC, which lead to the formation of a polyamide active layer
49 with multiscale heterogeneity and a large distribution of pore size²⁰⁻²⁴. Fundamental understanding
50 of the IP process continues to attract research interests due to the wide industrial application of
51 TFC-PA NF membranes^{10,25}. Extensive research efforts have been devoted to modulate the IP
52 process to achieve TFC-PA membranes with improved performance and desired properties¹⁸. For
53 example, the properties and performance of TFC-PA membranes can be controlled by using

54 different monomers and additives (including nanomaterials) and adjusting their concentrations^{26–}
55 ²⁹. Moreover, the environmental conditions for the fabrication also play an important role in
56 controlling the properties and performance of the resulting membranes^{11,30}.

57 One effective approach for modulating the IP process and the properties of the resulting TFC-
58 PA membranes is by adding surfactants^{31–33}. The roles of surfactants are multi-faceted and
59 dependent on the specific system. The most apparent role is to reduce the surface tension and
60 thereby promote the wetting of the support layer and stabilize the water/oil interface^{33–37}. It was
61 found in previous studies that the presence of surfactants has a substantial impact on the
62 morphology of the resulting PA layer formed from the polymerization between PIP and TMC,
63 which alters the membrane permeability³⁸. More recently, an additional role of surfactants in
64 regulating the cross-interface transport of PIP has been recently proposed³¹. Specifically, it has
65 been suggested that anionic surfactants, such as sodium dodecyl sulfate (SDS), which form a self-
66 assembled dynamic 2D network at the water-hexane interface, can promote the kinetics and
67 homogeneity of the PIP transport across the interface and results in a PA membrane with more
68 uniform pore sizes for precise molecular separation³¹.

69 In addition to these effects, some surfactants are also known to be good emulsifiers^{39–41}. The
70 effects of emulsifying surfactants on the IP process and the properties and performance of the
71 resulting TFC-PA membrane have not been systematically investigated. The theory on how the
72 chemical structure of surfactants affects their emulsifying behavior has been introduced by Griffin
73 who proposed to use a parameter called the hydrophile-lipophile balance (HLB) to estimate the
74 emulsification behavior of surfactants⁴¹. Surfactants with different HLB values have a different
75 affinity (or solubility) toward either the water or the oil phase, which results in different
76 emulsification behaviors. Specifically, surfactants with an HLB value from 8–16 (an approximate
77 range) are effective water in oil (w/o) emulsifiers, whereas surfactants with an HLB value of 3–6
78 are effective oil in water (o/w) emulsifiers^{40,41}. Effective emulsifiers of either kind (o/w or w/o)
79 will likely promote the formation of emulsions near the water/hexane interface and thus affect the
80 IP process, which in turn affects the properties and performance of the TFC-PA membranes.

81 In this study, we investigate the impacts of nonionic surfactants on the formation and properties
82 of the TFC-PA NF membranes. The nonionic surfactants investigated include Tween 80 (HLB=15)
83 and Span 80 (HLB=4.3). These two non-ionic surfactants were chosen because (1) they have the

proper HLBs as o/w and w/o emulsifiers, respectively, and (2) the absence of charge in these surfactants minimizes the complication of the surfactant charge effect in the IP and allows us to focus the analysis on the emulsification effect. We first fabricate the TFC-PA NF membranes with PIP and TMC using interfacial polymerization in the presence of either of the two surfactants and compare the resulting membranes to a reference TFC-PA NF membrane prepared without any surfactant. We then characterize the surface properties of these membranes and evaluate their NF performance in terms of water permeance and salt rejection. By comparing TFC-PA membranes fabricated with and without emulsifying agents, we aim to elucidate the impacts of emulsion formation on interfacial polymerization and the properties and NF performance of the resulting PA membranes.

94 MATERIAL AND METHODS

95 **Materials and Chemicals.** Piperazine (PIP, 99%), trimesoyl chloride (TMC, >98%), polysorbate 96 80 (Tween[®] 80, BioXtra, Mw ~1310), sorbitan oleate (Span[®] 80, Mw ~428), beta-carotene (\geq 93%, 97 oil soluble-dye), basic dye (meta phenylene blue bb c.i. 50255, water-soluble dye), glycerol (\geq 99%), anhydrous D-(+)-Glucose, sucrose (\geq 99.5%), D-(+)-Raffinose pentahydrate (\geq 98%), 99 Na₂SO₄ (\geq 99%), MgSO₄ (\geq 99.5%), MgCl₂ (\geq 99.99%), CaCl₂ (\geq 97%), NaCl (\geq 99%) were 100 purchased from Sigma Aldrich (St. Louis, MO) and were all used as received. Anhydrous N- 101 hexane and ethanol (HPLC) were purchased from Fisher Scientific. Polyester sulfone 102 ultrafiltration (NADIR UH050, MWCO 50000 Da) membrane was purchased from Microdyn- 103 Nadir (Germany).

104 **Preparation of polyamide nanofiltration membrane via interfacial polymerization** The 105 reference TFC-PA NF membrane was prepared using piperazine (PIP, 0.25% w/v aqueous solution) 106 and trimesoyl chloride (TMC, 0.2% w/v in n-hexane) on a commercial polyethersulfone (PES) 107 ultrafiltration (UF) membrane as the support layer via conventional interfacial polymerization (IP). 108 The concentration of PIP and TMC remained the same in the following discussion. In a standard 109 IP process, the PES UF support membrane was first placed on a glass plate and the surface of the 110 UF membrane was impregnated with the aqueous PIP solution for 30 s. The excess PIP solution 111 was then gently removed from the UF support membrane surface using a rubber roller. Next, a 112 hexane solution of TMC was poured onto the UF membrane surface and kept still for another 30 113 s, which resulted in the formation of a thin PA active layer over the PES support membrane surface.

114 The resulting TFC-PA membrane was rinsed with excessive n-hexane to remove unreacted TMC
115 from the surface and then cured in an oven at 60 °C for 30 min to increase the degree of crosslinking.
116 After curing, the TFC-PA membrane was stored in DI water at 4°C to facilitate the hydrolysis of
117 unreacted chloride groups in the polyamide network.

118 To investigate the effect of nonionic surfactants on interfacial polymerization and the resulting
119 TFC-PA membranes, the hydrophilic nonionic surfactant was added into the PIP solution for
120 impregnating the PES support layer, whereas the lipophilic nonionic surfactant was added in the
121 TMC hexane solution. The first nonionic surfactant, Tween 80, has a hydrophilic-lipophilic
122 balance (HLB) value of 15 and is thus considered a good oil-in-water emulsifier⁴⁰. The second
123 nonionic surfactant, Span 80, has an HLB value of 4.3 and is thus considered as good water-in-oil
124 emulsifier⁴¹. The concentration of Tween 80 (in water) and Span 80 (in hexane) vary from 0%
125 w/v to 0.5% w/v to evaluate the effect of surfactant concentration on the resulting polyamide
126 nanofiltration membrane.

127 **Membrane characterization.** We characterized the surface potentials of the TFC-PA NF
128 membranes using a streaming potential analyzer (SurPASS electrokinetic analyzer, Anton Paar,
129 Ashland, VA) with a background polyelectrolyte of 1mM KCl solution. We also measured the
130 water contact angle (WCA) of the TFC-PA membranes using an optical tensiometer (Theta Lite,
131 Biolin Scientific). Scanning electron microscope (SEM) imaging was performed to characterize
132 the surface morphology of the TFC-PA NF membranes using a high-resolution Zeiss Merlin SEM
133 equipped with a GEMINI II column with an accelerating voltage of 3 kV. All SEM membrane
134 samples were sputter-coated with a 5 nm gold coating to avoid the charging effect. X-ray
135 photoelectron spectrometry (XPS) was performed using an X-ray photoelectron spectrometer
136 (ESCALAB 250 Xi, Thermal Fisher Scientific) to obtain the surface elemental compositions of
137 polyamide active layers prepared from conventional IP and IP with nonionic surfactants. The
138 chemical structure of the TFC-PA NF membranes was also investigated using Fourier transform
139 infrared spectrometer (Bruker Tensor 27). Transmittance spectra were collected ranging from 800
140 to 4000 cm^{-1} at a resolution of 2 cm^{-1} for 256 scans.

141 To evaluate the pore size distribution of the TFC-PA NF membranes, we performed filtration
142 experiments with a series of neutral organic molecules (e.g., glycerol (92 Da), glucose (180 Da),
143 sucrose (342 Da), raffinose (504 Da)) using a custom cross-flow NF system. The feed

144 concentration was 200 ppm for all species and the applied pressure was 4 bar. We collected feed
145 and permeate samples and measured the total organic carbon (TOC) using a TOC analyzer (Aurora
146 Model 1030, OI Analytical, Inc.) to determine the organic concentrations of the feed and permeate
147 samples. The MWCO and pore size information of the TFC-PA NF membranes were calculated
148 using the rejection of the organic solutes. Specifically, the MWCO of the membrane is defined as
149 the molecular weight of solute with a rejection of 90%, whereas the mean pore size corresponds
150 to the Stokes radius of the neutral solute with a measured rejection rate of 50%. The pore size
151 distribution of the TFC-PA NF membrane is expressed as the geometric standard deviation of the
152 probability density function (PDF) curve (Equation 3), which is the ratio of the stokes radius with
153 a rejection of 84.13% to that with a rejection of 50%⁴².

$$\frac{dR(r_p)}{dr_p} = \frac{1}{r_p \ln \sigma_p \sqrt{2\pi}} \exp \left[-\frac{(\ln r_p - \ln \mu_p)^2}{2(\ln \sigma_p)^2} \right] \quad (3)$$

154 where μ_p is the mean pore size, σ_p is the geometric standard deviation of the PDF curve and r_p is
155 the Stokes radius of the organic solute. The Stokes radii of these molecules correlate with their
156 molecular weight⁴² (Equation 4):

$$\ln(r_p) = -1.496 + 0.465 \ln(MW) \quad (4)$$

157 where MW is the molecular weight of each organic solute. Based on this correlation, the Stokes
158 radii for glycerol, glucose, sucrose, and raffinose are 0.261, 0.359, 0.462, and 0.538 nm,
159 respectively.

160

161 **Dye-partitioning at water/hexane interface.** We performed dye partitioning experiments to
162 investigate how solutes in one phase partition to another phase in the presence of surfactants.
163 Specifically, we used a water-soluble dye (blue) in the aqueous solution to mimic the partitioning
164 of PIP from water into hexane during the IP process. We also used a lipid-soluble dye (yellow) in
165 the hexane to mimic the partitioning of TMC from hexane into the water during the IP. In all cases,
166 water was first placed in a beaker, and then hexane was on top of the water using a transfer pipet.
167 Each of the two phases (water or hexane) may or may not contain dyes or surfactants, with all the
168 experimental scenarios summarized in Table 1. The mixing behavior upon adding hexane to water
169 was recorded with both photos and videos.

170

171 **Table 1.** Summary of dye-partitioning experiments

Type of surfactant	Experiment No.	Components in each phase	
		Water phase	Hexane phase
Tween 80	1-1	None	Dye (yellow)
	1-2	Tween 80	Dye (yellow)
	1-3	Tween 80, dye (blue)	None
Span 80	2-1	Dye (blue)	None
	2-2	Dye (blue)	Span 80
	2-3	None	Span 80, dye (yellow)

172

173 **Nanofiltration performance evaluation.** The performance matrix including permeance and salt
 174 rejection of the TFC-PA NF membranes was evaluated using a custom-made crossflow filtration
 175 system (Figure S1). The crossflow system contains three stainless steel membrane testing cells
 176 connected in parallel. Three membranes were mounted into each of the three cells and tested
 177 simultaneously. Each cell has an active membrane area of 7.1 cm². The feed solution encounters a
 178 90° degree bend when it enters the cell inlet. The crossflow velocity was 2.5 cm s⁻¹ and the applied
 179 pressure was 4 bar. All membranes were compacted with deionized water overnight prior to any
 180 test with a salt solution. Membrane permeance and salt selectivity were evaluated with five types
 181 of common salt solutions (1000 ppm), including Na₂SO₄, MgSO₄, MgCl₂, CaCl₂, and NaCl. The
 182 solution temperature was maintained at 25 °C during the test. All measurements were carried out
 183 when the filtration process becomes stable. The permeance of the TFC-PA NF membrane, P (L
 184 m⁻² h⁻¹ bar⁻¹), was determined using the following equation:

$$P = \frac{J}{\Delta P} \quad (5)$$

185 where J is the volumetric flux of water (L m⁻² h⁻¹), and ΔP was the applied pressure (bar),
 186 respectively. The rejection of solute by the TFC-PA NF membrane was determined by measuring
 187 the steady-state electrical conductivity of the feed and permeate solution using the following
 188 equation.

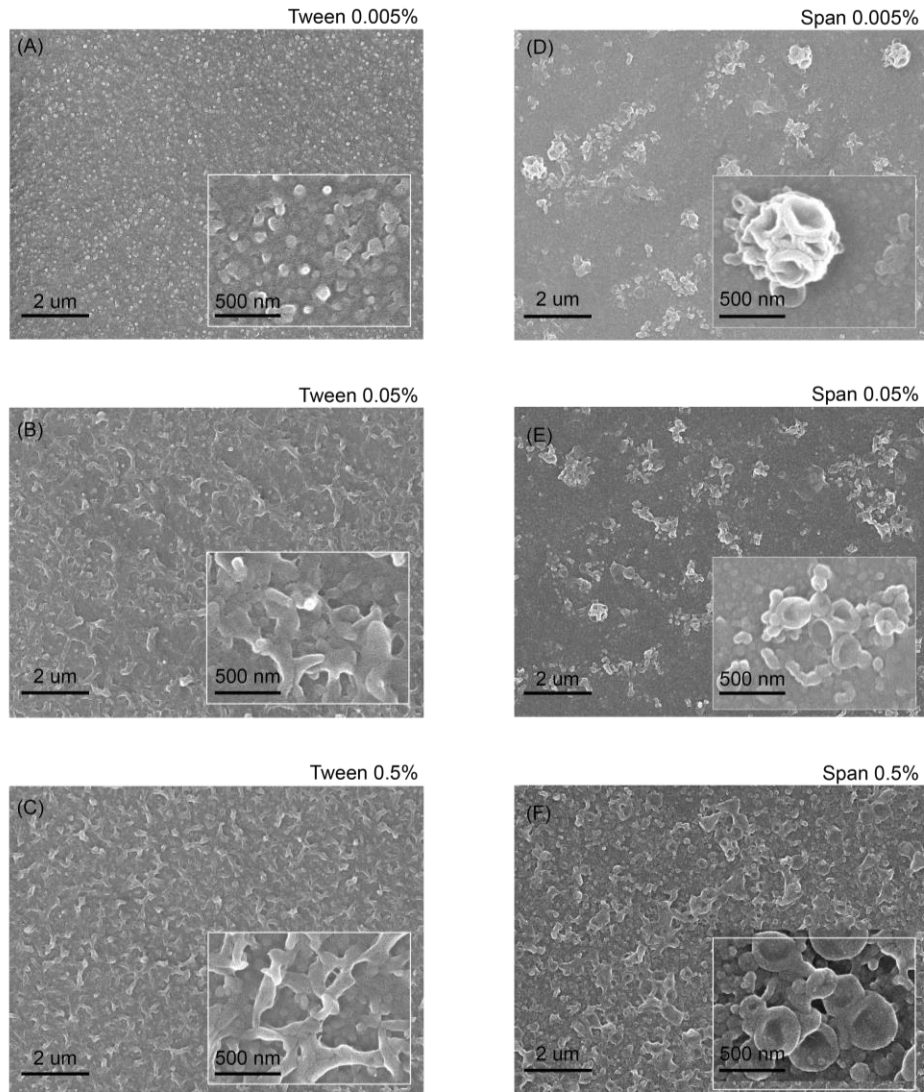
$$R = \left(1 - \frac{c_p}{c_f} \right) \times 100\% \quad (6)$$

189 where c_p and c_f are the solute concentration of permeate and feed solution, respectively,

190

191 **RESULTS AND DISCUSSION**

192 **Membrane surface morphology depends on surfactant type** The addition of hydrophilic and
193 lipophilic surfactants in IP has a substantial impact on the surface morphology of the resulting
194 TFC-PA NF membranes ([Figure 1](#)). As a baseline, the reference TFC-PA NF membrane prepared
195 from conventional IP (without any surfactant) has a relatively smooth surface ([Figure S2](#)). The
196 addition of hydrophilic nonionic surfactants (Tween 80) in the PIP solution leads to the formation
197 of nodular structures on the PA surface ([Figure 1A](#)). As the Tween 80 concentration increases from
198 0.005% w/v to 0.05% w/v in the PIP solution, the nodular structure transforms into a crumpled
199 structure ([Figure 1B](#)) and the density of the crumpled structure increases with increasing the Tween
200 80 concentration ([Figure 1C](#)). The formation of nodular and crumpled structures is attributed to
201 the enhanced wetting of the PIP solution on the PES UF substrate in the presence of Tween 80
202 ([Figure S3](#))³⁸. In comparison, the addition of lipophilic nonionic surfactants (Span 80) in the n-
203 hexane solution of TMC yields structures of deflated spheres on the PA surface ([Figure 1D](#)). The
204 areal number density of the deflated structures increases with increasing Span 80 concentration
205 ([Figure 1E](#)). At sufficiently high Span 80 concentration, these deflated spherical structures become
206 interconnected ([Figure 1F](#)).

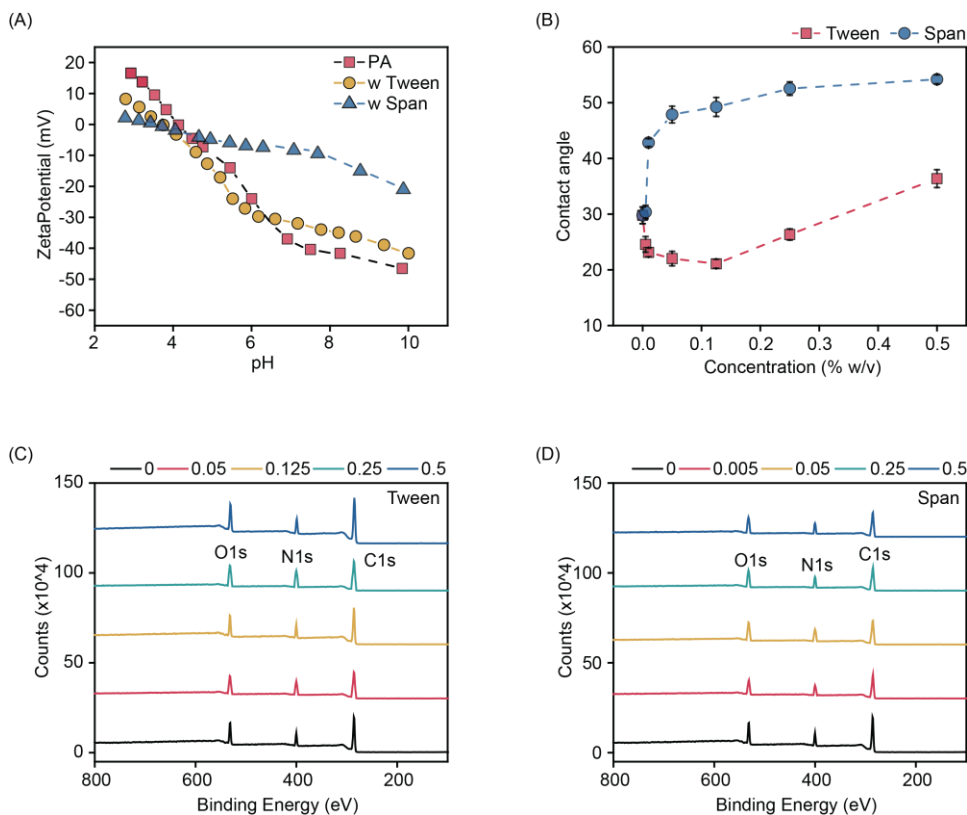


207

208 **Figure 1.** SEM images of the surface morphology of TFC-PA NF membranes formed via IP with
 209 the addition of (A, B, C) the hydrophilic nonionic surfactant (Tween 80) and (D, E, F) the lipophilic
 210 nonionic surfactant (Span 80) as a function of surfactant concentrations.

211 **Membrane surface properties depend on surfactant type** The streaming potential
 212 measurements reveal no discernable difference between the zeta potentials of the reference TFC-
 213 PA NF membrane prepared via conventional IP and the TFC-PA NF membrane prepared via IP
 214 with Tween 80 added in the PIP solution (Figure 2A), suggesting that the addition of Tween 80 in
 215 IP reaction did not alter the surface functional groups of the polyamide active layer. However, the
 216 addition of Span 80 in the TMC solution results in a noticeable reduction of the absolute values of
 217 the surface potential (i.e., the addition of Span 80 in IP reaction makes the TFC-PA membrane less
 218 charged) but without shifting the isoelectric point (IPE), which is likely caused by the reduction

219 of the areal density of the surface carboxylic groups due to the integration of the uncharged Span
 220 80 in the PA structure (including the surface). The addition of nonionic surfactants in the IP process
 221 also has a substantial impact on the wetting property of the resulting TFC-PA membrane (Figure
 222 2B). Specifically, the presence of Span 80 increased the water contact angle (WCA) systematically
 223 with a higher Span 80 concentration (in hexane) leading to a higher WCA. In comparison, the
 224 addition of Tween 80 has a less significant effect on the surface wetting property. Specifically,
 225 increasing the dosing concentration of Tween 80 (in water) first slightly reduced the WCA but
 226 then increased the WCA when the Tween 80 concentration exceeded 0.125% (w/v).



227
 228 **Figure 2.** (A) Surface streaming potential of TFC-PA membranes prepared from IP, and IP with
 229 the addition of the hydrophilic nonionic surfactant (Tween 80) and the lipophilic nonionic
 230 surfactant (Span 80). (B) Water contact angle of TFC-PA NF membrane formed via IP with the
 231 addition of the hydrophilic nonionic surfactant (Tween 80) and the lipophilic nonionic surfactant
 232 (Span 80) as a function of surfactant concentrations. XPS survey of polyamide active layer formed
 233 via IP with the addition of (C) the hydrophilic nonionic surfactant (Tween 80) and (D) the
 234 lipophilic nonionic surfactant (Span 80) as a function of surfactant concentrations.

235 The elemental composition of the TFC-PA surface is also dependent on both the type and
 236 concentration of the dosing surfactants. Analyzing the XPS spectra of the surface of the TFC-PA
 237 membranes fabricated using different conditions (Figure 2C, D) suggests the possible integration

238 of surfactants into the PA matrix. Specifically, the N/O ratio decreased systematically with an
 239 increasing Span 80 concentration (Table 2). When Tween 80 was the dosing agent, the N/O ratio
 240 first increased and then decreased when the concentration exceeded 0.125% (w/v) (Table 2). The
 241 integration of Tween 80 in the PA layer is further confirmed by the FT-IR analysis of the reference
 242 TFC-PA membrane and the TFC-PA membrane prepared from IP with Tween 80 (Figure S4).
 243 Specifically, the appearance of additional characteristic peaks at 1735 cm⁻¹ and 1098 cm⁻¹ is associated
 244 with the C=O stretching and the C-O-C stretching of the ester group^{43,44}.

245 **Table 2.** Elemental composition of the PA layer formed from IP with Tween 80 and Span 80

Membrane type	C(%)	N(%)	O(%)	N/O (%)
Reference (no surfactant added)	70.24	13.63	15.96	85.4
Tween 80	0.05% w/v	70.37	13.71	15.87
	0.125% w/v	71.04	13.37	15.24
	0.25% w/v	70.90	13.36	15.55
	0.5% w/v	71.38	12.68	15.81
Span 80	0.005% w/v	73.40	11.32	15.08
	0.05% w/v	69.52	12.40	18.08
	0.25% w/v	71.41	11.03	17.55
	0.5% w/v	73.62	10.00	16.38

246

247 Interestingly, the WCA (Figure 2B) negatively correlates with the N/O ratio (Table 1) in a
 248 semi-quantitative way for both Tween 80 and Span 80 (Figure S5). We note that while N/O ratio
 249 is often used in characterizing the degree of cross-linking in PA, it cannot be used for this purpose
 250 here due to the potential integration of non-ionic surfactants that may contribute substantially to
 251 the N/O ratio. The TFC-PA membranes prepared from IP with Span 80 exhibited an increase in
 252 surface hydrophobicity (WCA) and a decrease in N/O ratio even at an extremely low Span 80
 253 concentration (0.005% w/v). Increasing Span 80 concentration made the membrane more
 254 hydrophobic and reduced the N/O ratio because of the more Span 80 integrated into the PA matrix,
 255 which is also consistent with the observation of reduced absolute values of the surface potential
 256 for TFC-PA membrane prepared using Span. In comparison, very little Tween 80 integration in
 257 the polyamide matrix was observed at low Tween 80 concentrations (below 0.25% w/v), as the

258 N/O ratio remains nearly constant. The slight decrease in WCA may come from the increase in
259 surface roughness ([Figure 1A-C](#), [Figure S2](#)), as consistent with Wenzel's theory⁴⁵.

260 The primary difference between Span 80 and Tween 80 in their effectiveness in altering the
261 PA composition and properties can be explained by the fact that Span 80 was present in the hexane
262 phase where PA forms. While the formation of PA is referred to as "interfacial polymerization",
263 multiple previous studies have suggested that the polymerization occurs in the "hexane side" of
264 the interface^{20,21,23}. Because Span 80 is soluble in hexane and was dosed in hexane, they are likely
265 integrated into the PA layer formed in the hexane phase. In comparison, Tween 80 is barely soluble
266 in hexane and was added to the aqueous solution. For this reason, it is substantially less likely that
267 Tween 80 molecules could be integrated into the PA layer, especially considering that IP is a rather
268 rapid and self-terminating process. Based on both the results of WCA and N/O values, a small
269 degree of Tween 80 integration was observed only when the Tween 80 concentration exceeded
270 0.25% w/v. The above explanation on the effect of the surfactants in PA membrane properties
271 focuses primarily on whether the surfactant molecules exist in the hexane phase where PA is
272 formed. However, surfactants may have an additional effect via the formation of emulsions, which
273 will be discussed in the following section.

274 **Emulsions as vehicles and microreactors** Like all other surfactants, Tween 80 also promotes
275 better wetting of the support layer (Supporting Information [Figure S3](#)), and both Tween 80 and
276 Span 80 reduces the interfacial tension between water and hexane ([Figure 3A](#)). However, Tween
277 80 and Span 80 differ from some common surfactants in that their HLB values fall into the ranges
278 of effective emulsifiers³⁹. For example, Tween 80 (HLB~15) is a good oil-in-water (o/w)
279 emulsifier (HLB range: 8-18), whereas Span 80 (HLB~4.3) is a good water-in-oil (w/o) emulsifier
280 (HLB range: 4-6). To illustrate the effectiveness of these surfactants in emulsification, we
281 performed experiments to show the stability of the oil/water interface when the surfactants are
282 added into one of the two phases. Specifically, the oil phase was dosed with an orange, water-
283 insoluble dye (beta carotene) and the water phase was dosed with a blue, oil-insoluble dye (meta
284 phenylene blue) to clearly show the oil/water interface.

285 With no surfactants added, the water/hexane interface was relatively clear and stable ([Figure](#)
286 [3B](#), [E](#)). No oil dye partitions into the clear water phase ([Figure 3B](#)), and no water dye partitions
287 into the clear oil phase ([Figure 3E](#)). When Tween 80 was added into the clear (undyed) water phase

which was put into contact with the hexane phase containing orange dye, the water phase became muddy and orange, which indicates the formation of o/w emulsion containing the orange dye (Figure 3C). Similarly, when Span 80 was added into the transparent hexane phase which was put into contact with the blue-dyed water phase, the hexane phase also showed clear evidence of the formation of w/o emulsions containing the blue dye (Figure 3F).

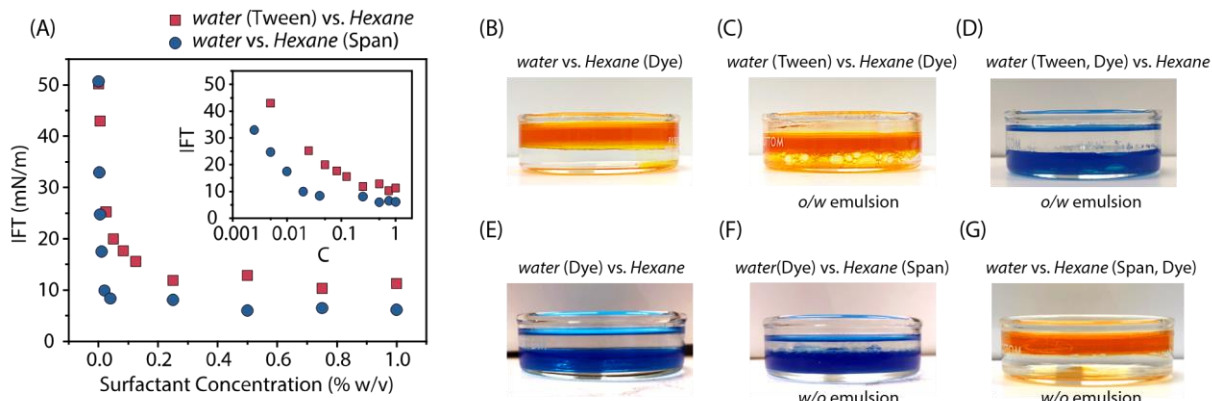
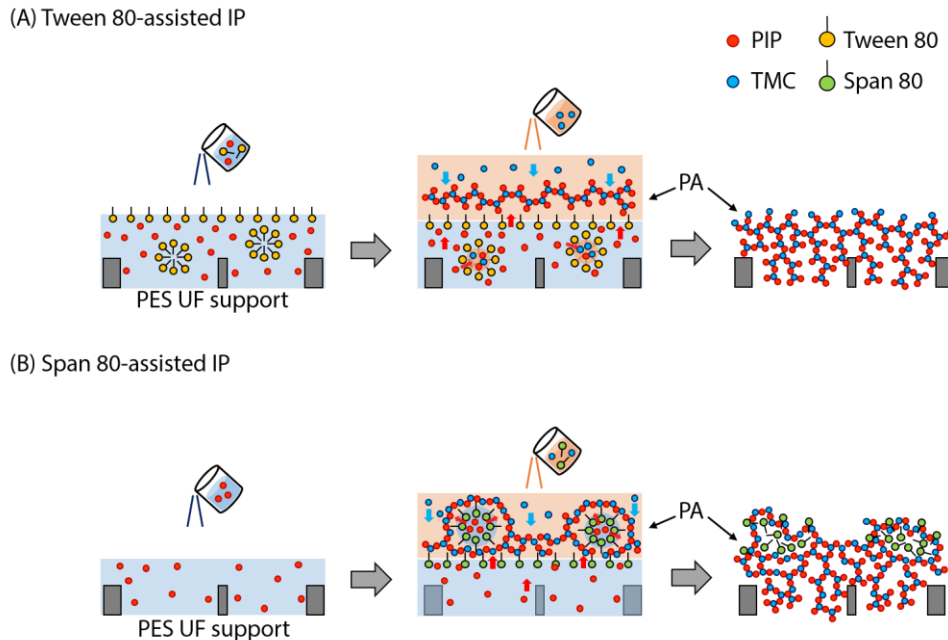


Figure 3. (A) Interfacial surface tension of water and hexane as a function of Tween 80 concentration in water (red square) or Span 80 concentration in hexane (blue circle). Demonstration of the presence of Tween 80 in water leading to the formation of oil-in-water emulsion upon mixing of water and hexane: (B) control experiment: when tween 80 is absent, no emulsion (yellow color) is observed in water. (C) the presence of Tween 80 results in the formation of oil-in-water emulsion (yellow bubbles) in water. (D) control experiment: Tween 80 does not lead to the formation of water-in-oil emulsion (no blue color) in hexane. Demonstration of the presence of Span 80 in hexane leading to the formation of water-in-oil emulsion upon mixing of water and hexane: (E) control experiment: when Span 80 is absent, no color (emulsion) is observed in hexane. (F) The presence of Span 80 results in the formation of water-in-oil emulsion (blue bubbles) in hexane. (G) control experiment: Span 80 does not lead to the formation of oil-in-water emulsion (no yellow color) in water.

In the experiments shown in Figure 3C, F, the dyes, and the surfactants were added into different phases, which does not clearly show if emulsions also formed in the dyed phase. Therefore, we performed additional experiments where dyes and surfactants were added in the same phase. Specifically, when both Tween 80 and water-soluble dye were added into water, no formation of the blue emulsion was observed in the clear oil phase (Figure 3D). The absence of emulsification in the oil phase is attributable to the fact that Tween 80, being a good o/w emulsifier, is a poor w/o emulsifier. Similarly, when both Span 80 and the oil-soluble dye were added into the oil phase, no o/w emulsion was observed in the water phase (Figure 3G), because Span 80, though being an effective w/o emulsifier, is a poor o/w emulsifier.

315 The emulsification behaviors in the presence of non-ionic surfactants as illustrated using dyed
316 solutions provide important insights into how interfacial polymerization (IP) can be affected by
317 these surfactants. Specifically, we consider the effect of monomer transporting via emulsions
318 containing those monomers, i.e., the emulsions serve as “vehicles” to bring the monomers into
319 another phase. For example, when Tween 80 was added into the PIP solution, o/w emulsions
320 formed in the aqueous solution brought the emulsified oil droplets containing TMC into the water
321 phase. These emulsified oil droplets served as microreactors for local interfacial polymerization
322 that led to the formation of short PA fragments. These disconnected segments forming in the water
323 phase were unlikely integrated into the continuous PA layer formed on the hexane side of the
324 water/hexane interface. Instead, these segments were likely subject to fast hydrolysis, became
325 embedded underneath the PA active layer, and had limited impact on the properties of the PA layer.

326 In fact, the streaming potential measurements reveal almost no difference in surface potential
327 between the PA layers formed with and without Tween 80 ([Figure 2A](#)). The presence of Tween
328 80 has a relatively small impact (as compared to Span 80 to be discussed) on the WCA and
329 elemental composition of the PA layer ([Figure 2B, C and Table 2](#)), which is likely attributable to
330 the integration of Tween 80 in the PA layer. We note that the integration of a small amount of
331 Tween 80 does not affect the surface potential of the PA layer because Tween 80 does not partition
332 into the hexane phase and is thus not present on and near the surface of the resulting PA layer.
333 Similarly, the changes in WCA and elemental composition were hardly observed if oil-insoluble
334 and non-emulsifying surfactants (e.g., SDS or SDBS) were used ³¹. These observations are all
335 consistent with the above hypothesis regarding how Tween 80 may affect the PA formation. Lastly,
336 the emergence of the nodular and crumpled structures ([Figure 1A-C](#)) results from the improved
337 wetting of the PES substrate by the surfactant-dosed PIP solution, which has been well elaborated
338 in the work by Niu et al.³⁸



339

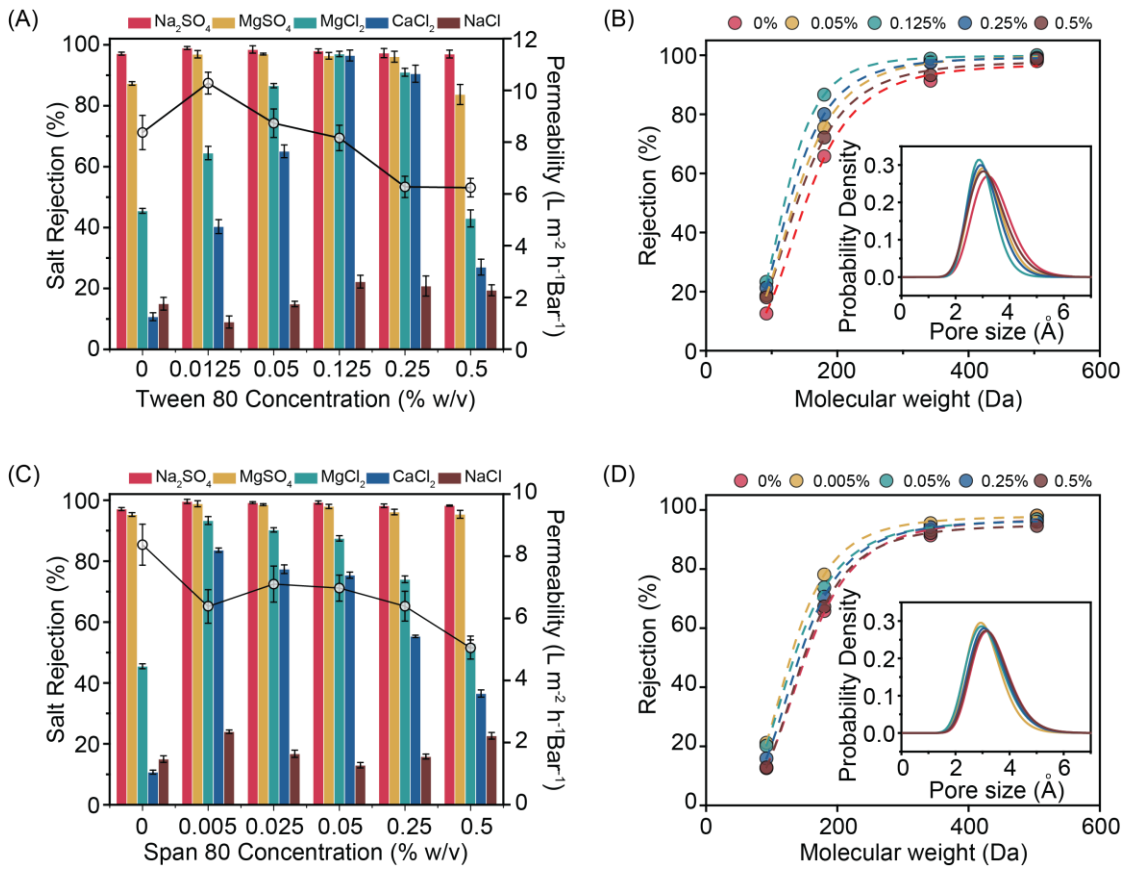
340 **Figure 4.** Schematic illustration of the polyamide active layer formation via IP with the addition
 341 of (A) the hydrophilic nonionic surfactant (Tween 80) and (B) the lipophilic nonionic surfactant
 342 (Span 80).

343 In comparison, adding Span 80 into the hexane TMC solution has a very different impact on
 344 interfacial polymerization. As Span 80 is a highly effective w/o emulsifier, PIP encapsulated in
 345 water-in-hexane (w/o) emulsions transport to the hexane phase via the “vehicle effect”. The
 346 emulsion-facilitated transport of PIP adds to the trans-interface diffusion of PIP from water to
 347 hexane. These w/o emulsions also serve as microreactors for interfacial polymerization. In this
 348 case, however, the PA formed around the emulsified water droplets because PA tends to form in
 349 the hexane side of the water/hexane interface. These PA fragments are less susceptible to
 350 hydrolysis as they are in the hexane phase and are thus given the opportunity to continue to react
 351 with other PA fragments forming from the reaction between TMC and the PIP diffusing across the
 352 interface between the bulk water and bulk hexane. Eventually, these “PA vesicles” forming at the
 353 w/o emulsion interface merged with the PA film forming at the interface between the bulk phases.
 354 When the PA membrane was dried, the evaporation of water inside these vesicles led to the
 355 formation of collapsed vesicles as observed in **Figure 1D-F**. In this case, the Span 80 surfactants
 356 were trapped in the collapsed PA layers and contributed substantially to the chemical composition
 357 of the PA layer (**Table 1**) and the physical properties of the PA layers such as surface potential
 358 (**Figure 2A**) and WCA (**Figure 2B**).

359 **Membrane performance and pore structure.** The additions of Tween 80 in water and Span 80
360 in hexane resulted in distinct membrane performance. When Tween 80 was added into the aqueous
361 phase, the membrane permeability slightly increased at low Tween 80 concentration due to the
362 creation of crumpled structure on the membrane surface which increased the specific surface area,
363 then decreased as the pore size of the TFC-PA membranes decreased at high Tween 80
364 concentrations ([Figure 5A](#)). The measured salt rejection of the TFC-PA NF membranes increased
365 when Tween 80 concentration increased from 0% w/v to 0.125% w/v ([Figure 5A](#)). But when the
366 Tween 80 concentration exceeded 0.5% w/v, the salt rejections for several salts (except Na_2SO_4)
367 declined. The initial increase of the salt rejection was attributable to a reduction of the molecular
368 weight cut-off (MWCO) of the TFC-PA membranes prepared in the presence of Tween 80 ([Figure](#)
369 [5B and inset](#)). In particular, the TFC-PA membranes prepared with a Tween 80 concentration of
370 0.125% w/v exhibited a remarkable performance for separating divalent and multivalent ions (e.g.,
371 Zn^{2+} , Mg^{2+} , SO_4^{2-} , $\text{Fe}(\text{CN})_6^{3-}$, etc.) from monovalent salt (K^+ , Na^+ , NO_3^- , etc.) ([Figure S6](#)).

372 This enhancement in the solute separation precision by Tween 80 is similar to what has been
373 observed in surfactant assembly-regulated interfacial polymerization (SARIP) using SDS³¹.
374 Similar to the sulfate group in SDS, Tween 80 has abundant hydroxyl groups on its hydrophilic
375 end, which can attract the positively charged PIP molecules. Also, the self-assembled Tween 80
376 network at the water-hexane interface regulates the trans-interface diffusion of PIP from the water
377 phase to the hexane phase and thereby improves the homogeneity of the pore size distribution of
378 the resulting PA membrane ([Table 3](#)). However, when the Tween 80 concentration reached 0.5%
379 w/v, the separation performance became compromised as the rejections of divalent cations became
380 substantially lower ([Figure 5A](#)) and the MWCO of the membrane became larger ([Figure 5B](#)).

381 The deterioration in performance at a relatively high Tween 80 concentration is likely
382 attributable to the integration of Tween 80 molecules in the PA active layer as indicated by both
383 the measured WCA ([Figure 5B](#)) and active layer composition ([Table 2](#)). While the exact
384 mechanism of Tween 80 integration into the PA network is unclear, we speculate that such an
385 integration is attributable to both (1) the van der Waals interaction between the hydrocarbon chain
386 of Tween 80 and PA and (2) the hydrogen bond between the hydroxyl groups of Tween 80 and the
387 amine groups of the PIP (that are diffusing across the interface) and of the formed PA segments.



388

389 **Figure 5.** (A) Pure water permeability (line) and rejection of different salts (columns) by the TFC-PA
390 membranes (prepared by adding Tween 80 in the PIP solution) as a function of Tween 80 concentration.
391 (B) Rejection of uncharged organic molecules including glycerol, glucose, sucrose, and raffinose by TFC-
392 PA membranes prepared using different Tween 80 concentrations. Inset: pore size distribution of the PA-
393 TFC NF membranes as derived from the rejection curves of uncharged organic molecules. (C) Pure water
394 permeability (line) and rejection of different salts (columns) by the TFC-PA membranes (prepared by
395 adding Span 80 in the PIP solution) as a function of Span 80 concentration. (D) Rejection of uncharged
396 organic molecules including glycerol, glucose, sucrose, and raffinose by TFC-PA membranes prepared
397 using different Span 80 concentrations. Inset: pore size distribution of the PA-TFC NF membranes as
398 derived from the rejection curves of uncharged organic molecules. All measurements were carried out at
399 an applied pressure of 4 bar. Rejection and flux data are reported as the average of three runs, and the error
400 bars represent the standard deviation.

401

402

403

404

405

406

407

408 **Table 3.** Mean pore size and pore size distribution of the PA layers formed from IP with Tween
 409 80 (in water) and Span 80 (in hexane).

Membrane type		Mean pore size (Å)	Pore size distribution
Reference (no surfactant added)		3.312	1.238
Tween 80	0.05%	3.126	1.222
	0.125%	2.956	1.189
	0.25%	3.046	1.217
	0.5%	3.175	1.245
Span 80	0.005%	3.064	1.233
	0.05%	3.124	1.258
	0.25%	3.209	1.241
	0.5%	3.28	1.243

410
 411 Adding a small concentration of Span 80 resulted in a substantial improvement of divalent
 412 cation rejection (Figure 5C), which is again likely attributable to the mechanism of SARIP. It
 413 requires a lower concentration of Span 80 than Tween 80 to induce similar enhancement in divalent
 414 cation rejection, which is likely because Span 80 has a higher surface excess concentration than
 415 Tween 80 (Figure 3A) and can thus form a denser interfacial surfactant network than Tween 80 at
 416 the same bulk concentration⁴⁶. However, as Span 80 molecules were integrated into the PA
 417 network by an increasing extent with heightened Span 80 concentration, the rejection of divalent
 418 cations systematically decreased. Because of the hydrophobic nature of Span 80, the implantation
 419 of Span 80 inside the polyamide network led to a reduction of the membrane permeability due to
 420 the reduced surface hydrophilicity (Figure 2B). The changes of MWCO and pore size distribution
 421 as a function of Span 80 concentration also follow the same trend as that for divalent cation
 422 rejection (Figure 5D) and are in general consistent with the dependence of membrane properties
 423 (water contact angles and elemental composition) on the Span 80 concentration (Figure 2B, Table
 424 2). In other words, the addition of Span 80 has competing effects of SARIP and surfactant
 425 integration (into the PA network), with the former having a positive impact and the later having a
 426 negative impact on the membrane pore size (Table 3), rejection of divalent cations and on
 427 achieving precise selective ion separation.

428

429 **CONCLUSION**

430 We show in this comparative study how the addition of emulsifying nonionic surfactants in the IP
431 process can affect the properties and nanofiltration performance of the resulting TFC-PA
432 membranes. Our experimental results suggest that in addition to the known effects of surfactants
433 such as SARIP and improved wetting of the supporting layer, the formation of emulsions also has
434 interesting impacts on the IP process. In particular, the addition into the hexane phase Span 80,
435 which is an effective w/o emulsifier, has a substantial impact on the various properties
436 (morphology, surface potential, wetting properties, and composition) and the NF performance of
437 the resulting TFC-PA membranes via both the “vehicle effect” and integration of surfactants into
438 the PA layer. Whereas, the addition of a hydrophilic nonionic surfactant, Tween 80, as an effective
439 o/w emulsifier, reveals a qualitatively similar effect on the structure-performance properties of the
440 resulting TFC-PA membranes as an anionic surfactant, SDS. This finding not only demonstrates
441 the mechanism of nonionic surfactant-mediated IP, but also provides additional guidance for the
442 surfactant selection to tailor the structure and performance of TFC-PA NF membranes.

443 **ACKNOWLEDGMENTS**

444 This work is supported by the National Natural Science Funds for Distinguished Young Scholar
445 (51625306), the National Natural Science Foundation of China (21988102). S.Lin also
446 acknowledges the partial supports from U.S. National Science Foundation (CBET-2017998).

447 **ASSOCIATED CONTENT**

448 **Supporting Information**

449 Additional figures: Figure S1, Custom-made crossflow NF testing system. Figure S2, SEM image
450 of the surface morphology of TFC-PA NF membranes formed via conventional IP; Figure S3,
451 Contact angle of PIP-Tween 80 aqueous solution on the PES UF substrate as a function of Tween
452 80 concentration.; Figure S4, FT-IR spectrum of the reference TFC-PA membrane prepared from
453 conventional IP and the TFC-PA membrane prepared from IP with Tween 80 (Concentration of
454 Tween 80 is 0.125% w/v); Figure S5, Water contact angle and the N/O ratio of the TFC-PA NF
455 membrane formed via IP with the addition of the hydrophilic nonionic surfactant (Tween 80) and
456 the lipophilic nonionic surfactant (Span 80) as a function of surfactant concentrations; Figure S6,
457 Selectivity of different solutes as a function of Stokes radii for the PA-TFC NF membrane prepared
458 via IP with 0.125% w/v Tween 80 in PIP solution.

459 **AUTHOR INFORMATION**

460 **Corresponding authors**

461 Yuzhang Zhu - i-Lab and CAS Center for Excellence in Nanoscience, Suzhou Institute of Nano-
462 Tech and Nano-Bionics, Chinese Academy of Sciences, Suzhou 215123, P.R. China;
463 Email: yzzhu2011@sinano.ac.cn

464 Jian Jin - i-Lab and CAS Center for Excellence in Nanoscience, Suzhou Institute of Nano-Tech
465 and Nano-Bionics, Chinese Academy of Sciences, Suzhou 215123, P.R. China; College of
466 Chemistry, Chemical Engineering and Materials Science, Soochow University, Suzhou 215123,
467 P. R. China; Email: jjin2009@sinano.ac.cn;

468 Shihong Lin - Department of Civil and Environmental Engineering, Vanderbilt University,
469 Nashville, TN 37235-1831, USA; Interdisciplinary Material Science Program, Vanderbilt
470 University, Nashville, TN 37235, USA; Email: shihong.lin@vanderbilt.edu

471 **Authors**

472 Yuanzhe Liang - i-Lab and CAS Center for Excellence in Nanoscience, Suzhou Institute of Nano-
473 Tech and Nano-Bionics, Chinese Academy of Sciences, Suzhou 215123, P.R. China; Department
474 of Civil and Environmental Engineering, Vanderbilt University, Nashville, TN 37235-1831, USA;
475 Interdisciplinary Material Science Program, Vanderbilt University, Nashville, TN 37235, USA;

476 Xiangxiu Teng - i-Lab and CAS Center for Excellence in Nanoscience, Suzhou Institute of Nano-
477 Tech and Nano-Bionics, Chinese Academy of Sciences, Suzhou 215123, P.R. China;

478 Rui Chen - Department of Civil and Environmental Engineering, Vanderbilt University, Nashville,
479 TN 37235-1831, USA;

480 **Notes**

481 The authors declare no competing financial interest.

482 **REFERENCES**

483 (1) Elimelech, M.; Phillip, W. A. The Future of Seawater Desalination: Energy, Technology, and the
484 Environment. *Science (80-)*. **2011**, 333 (6043), 712–717.
485 <https://doi.org/10.1126/science.1200488>.

486 (2) Bohn, P. W.; Elimelech, M.; Georgiadis, J. G.; Mariñas, B. J.; Mayes, A. M.; Mayes, A. M. *Science*

487 and Technology for Water Purification in the Coming Decades. In *Nanoscience and Technology: A*
488 *Collection of Reviews from Nature Journals*; World Scientific, 2009; pp 337–346.
489 https://doi.org/10.1142/9789814287005_0035.

490 (3) Li, R.; Shi, Y.; Shi, L.; Alsaedi, M.; Wang, P. Harvesting Water from Air: Using Anhydrous Salt with
491 Sunlight. *Environ. Sci. Technol.* **2018**, *52* (9), 5398–5406.
492 <https://doi.org/10.1021/acs.est.7b06373>.

493 (4) Wang, R.; Zimmerman, J. B. Economic and Environmental Assessment of Office Building
494 Rainwater Harvesting Systems in Various U.S. Cities. *Environ. Sci. Technol.* **2015**, *49* (3), 1768–
495 1778. <https://doi.org/10.1021/es5046887>.

496 (5) Misra, A. K. Climate Change and Challenges of Water and Food Security. *Int. J. Sustain. Built
497 Environ.* **2014**, *3* (1), 153–165. <https://doi.org/10.1016/j.ijsbe.2014.04.006>.

498 (6) Tang, C. Y.; Yang, Z.; Guo, H.; Wen, J. J.; Nghiem, L. D.; Cornelissen, E. Potable Water Reuse
499 through Advanced Membrane Technology. *Environ. Sci. Technol.* **2018**, *52* (18), 10215–10223.
500 <https://doi.org/10.1021/acs.est.8b00562>.

501 (7) Fane, A. G.; Wang, R.; Hu, M. X. Synthetic Membranes for Water Purification: Status and Future.
502 *Angew. Chemie - Int. Ed.* **2015**, *54* (11), 3368–3386. <https://doi.org/10.1002/anie.201409783>.

503 (8) Werber, J. R.; Osuji, C. O.; Elimelech, M. Materials for Next-Generation Desalination and Water
504 Purification Membranes. *Nature Reviews Materials*. 2016.
505 <https://doi.org/10.1038/natrevmats.2016.18>.

506 (9) Mohammad, A. W.; Teow, Y. H.; Ang, W. L.; Chung, Y. T.; Oatley-Radcliffe, D. L.; Hilal, N.
507 Nanofiltration Membranes Review: Recent Advances and Future Prospects. *Desalination* **2015**,
508 356, 226–254. <https://doi.org/10.1016/j.desal.2014.10.043>.

509 (10) Hilal, N.; Al-Zoubi, H.; Darwish, N. A.; Mohammad, A. W.; Abu Arabi, M. A Comprehensive Review
510 of Nanofiltration Membranes: Treatment, Pretreatment, Modelling, and Atomic Force
511 Microscopy. *Desalination* **2004**, *170* (3), 281–308. <https://doi.org/10.1016/j.desal.2004.01.007>.

512 (11) Petersen, R. J. Composite Reverse Osmosis and Nanofiltration Membranes. *Journal of Membrane
513 Science*. Elsevier August 12, 1993, pp 81–150. [https://doi.org/10.1016/0376-7388\(93\)80014-O](https://doi.org/10.1016/0376-7388(93)80014-O).

514 (12) Van Der Bruggen, B.; Vandecasteele, C. Removal of Pollutants from Surface Water and

515 Groundwater by Nanofiltration: Overview of Possible Applications in the Drinking Water Industry.
516 *Environ. Pollut.* **2003**, *122* (3), 435–445. [https://doi.org/10.1016/S0269-7491\(02\)00308-1](https://doi.org/10.1016/S0269-7491(02)00308-1).

517 (13) Fernandes, P. A.; Natália, M.; Cordeiro, D. S.; Gomes, J. A. N. F. Influence of Ion Size and Charge in
518 Ion Transfer Processes Across a Liquid|Liquid Interface. *J. Phys. Chem. B* **2000**, *104* (10), 2278–
519 2286. <https://doi.org/10.1021/jp993045z>.

520 (14) Cadotte, J. E.; Petersen, R. J.; Larson, R. E.; Erickson, E. E. A New Thin-Film Composite Seawater
521 Reverse Osmosis Membrane. *Desalination* **1980**, *32* (C), 25–31. [https://doi.org/10.1016/S0011-9164\(00\)86003-8](https://doi.org/10.1016/S0011-9164(00)86003-8).

522 (15) Cadotte, J. E.; King, R. S.; Majerle, R. J.; Petersen, R. J. Interfacial Synthesis in the Preparation of
523 Reverse Osmosis Membranes. *J. Macromol. Sci. Part A - Chem.* **1981**, *15* (5), 727–755.
524 <https://doi.org/10.1080/00222338108056764>.

525 (16) Wang, Z.; Wang, Z.; Lin, S.; Jin, H.; Gao, S.; Zhu, Y.; Jin, J. Nanoparticle-Templated Nanofiltration
526 Membranes for Ultrahigh Performance Desalination. *Nat. Commun.* **2018**, *9* (1), 1–9.
527 <https://doi.org/10.1038/s41467-018-04467-3>.

528 (17) Paul, M.; Jons, S. D. Chemistry and Fabrication of Polymeric Nanofiltration Membranes: A
529 Review. *Polymer (Guildf.)* **2016**, *103*, 417–456. <https://doi.org/10.1016/j.polymer.2016.07.085>.

530 (18) Ng, L. Y.; Mohammad, A. W.; Ng, C. Y. A Review on Nanofiltration Membrane Fabrication and
531 Modification Using Polyelectrolytes: Effective Ways to Develop Membrane Selective Barriers and
532 Rejection Capability. *Adv. Colloid Interface Sci.* **2013**, *197–198*, 85–107.
533 <https://doi.org/10.1016/j.cis.2013.04.004>.

534 (19) Lau, W. J.; Ismail, A. F.; Misdan, N.; Kassim, M. A. A Recent Progress in Thin Film Composite
535 Membrane: A Review. *Desalination* **2012**, *287*, 190–199.
536 <https://doi.org/10.1016/j.desal.2011.04.004>.

537 (20) Wittbecker, E. L.; Morgan, P. W. Interfacial Polycondensation. I. *J. Polym. Sci.* **1959**, *40* (137),
538 289–297.

539 (21) Morgan, P. W. Interfacial Polycondensation. 11. Fundamentals of Polymer Formation. *J. Polym.*
540 *Sci.* **1959**, *327* (September 1958).

541 (22) Freger, V. Nanoscale Heterogeneity of Polyamide Membranes Formed by Interfacial

543 Polymerization. *Langmuir* **2003**, *19* (11), 4791–4797. <https://doi.org/10.1021/la020920q>.

544 (23) Freger, V. Kinetics of Film Formation by Interfacial Polycondensation. *Langmuir* **2005**, *21* (5),
545 1884–1894. <https://doi.org/10.1021/la048085v>.

546 (24) Zhang, H.; He, Q.; Luo, J.; Wan, Y.; Darling, S. B. Sharpening Nanofiltration: Strategies for
547 Enhanced Membrane Selectivity. *ACS Appl. Mater. Interfaces* **2020**, *12* (36), 39948–39966.
548 <https://doi.org/10.1021/acsami.0c11136>.

549 (25) Marchetti, P.; Jimenez Solomon, M. F.; Szekely, G.; Livingston, A. G. Molecular Separation with
550 Organic Solvent Nanofiltration: A Critical Review. *Chem. Rev.* **2014**, *114* (21), 10735–10806.
551 <https://doi.org/10.1021/cr500006j>.

552 (26) Saha, N. K.; Joshi, S. V. Performance Evaluation of Thin Film Composite Polyamide Nanofiltration
553 Membrane with Variation in Monomer Type. *J. Memb. Sci.* **2009**, *342* (1–2), 60–69.
554 <https://doi.org/10.1016/j.memsci.2009.06.025>.

555 (27) Rajaeian, B.; Rahimpour, A.; Tade, M. O.; Liu, S. Fabrication and Characterization of Polyamide
556 Thin Film Nanocomposite (TFN) Nanofiltration Membrane Impregnated with TiO₂ Nanoparticles.
557 *Desalination* **2013**, *313*, 176–188. <https://doi.org/10.1016/j.desal.2012.12.012>.

558 (28) Lee, S. Y.; Kim, H. J.; Patel, R.; Im, S. J.; Kim, J. H.; Min, B. R. Silver Nanoparticles Immobilized on
559 Thin Film Composite Polyamide Membrane: Characterization, Nanofiltration, Antifouling
560 Properties. *Polym. Adv. Technol.* **2007**, *18* (7), 562–568. <https://doi.org/10.1002/pat.918>.

561 (29) Yang, Z.; Guo, H.; Yao, Z. K.; Mei, Y.; Tang, C. Y. Hydrophilic Silver Nanoparticles Induce Selective
562 Nanochannels in Thin Film Nanocomposite Polyamide Membranes. *Environ. Sci. Technol.* **2019**,
563 *53* (9), 5301–5308. <https://doi.org/10.1021/acs.est.9b00473>.

564 (30) Ma, X. H.; Yao, Z. K.; Yang, Z.; Guo, H.; Xu, Z. L.; Tang, C. Y.; Elimelech, M. Nanofoaming of
565 Polyamide Desalination Membranes to Tune Permeability and Selectivity. *Environ. Sci. Technol.*
566 *Lett.* **2018**, *5* (2), 123–130. <https://doi.org/10.1021/acs.estlett.8b00016>.

567 (31) Liang, Y.; Zhu, Y.; Liu, C.; Lee, K. R.; Hung, W. S.; Wang, Z.; Li, Y.; Elimelech, M.; Jin, J.; Lin, S.
568 Polyamide Nanofiltration Membrane with Highly Uniform Sub-Nanometre Pores for Sub-1 Å
569 Precision Separation. *Nat. Commun.* **2020**, *11* (1), 1–9. [https://doi.org/10.1038/s41467-020-15771-2](https://doi.org/10.1038/s41467-020-
570 15771-2).

571 (32) Bojarska, M.; Gierycz, P.; Religa, P.; Kowalik-Klimczak, A. The Effect of Anionic Surfactant on the
572 Surface Structure of Nanofiltration Membranes. *Challenges Mod. Technol.* **2014**, *5* (2), 33–38.

573 (33) Mansourpanah, Y.; Madaeni, S. S.; Rahimpour, A. Fabrication and Development of Interfacial
574 Polymerized Thin-Film Composite Nanofiltration Membrane Using Different Surfactants in
575 Organic Phase; Study of Morphology and Performance. *J. Memb. Sci.* **2009**, *343* (1–2), 219–228.
576 <https://doi.org/10.1016/j.memsci.2009.07.033>.

577 (34) Mansourpanah, Y.; Alizadeh, K.; Madaeni, S. S.; Rahimpour, A.; Soltani Afarani, H. Using Different
578 Surfactants for Changing the Properties of Poly(Piperazineamide) TFC Nanofiltration Membranes.
579 *Desalination* **2011**, *271* (1–3), 169–177. <https://doi.org/10.1016/j.desal.2010.12.026>.

580 (35) Duong, P. H. H.; Anjum, D. H.; Peinemann, K. V.; Nunes, S. P. Thin Porphyrin Composite
581 Membranes with Enhanced Organic Solvent Transport. *J. Memb. Sci.* **2018**, *563*, 684–693.
582 <https://doi.org/10.1016/j.memsci.2018.04.038>.

583 (36) Cui, Y.; Liu, X. Y.; Chung, T. S. Ultrathin Polyamide Membranes Fabricated from Free-Standing
584 Interfacial Polymerization: Synthesis, Modifications, and Post-Treatment. *Ind. Eng. Chem. Res.*
585 **2017**, *56* (2), 513–523. <https://doi.org/10.1021/acs.iecr.6b04283>.

586 (37) Azarteimour, F.; Amirinejad, M.; Parvini, M.; Yarvali, M. Organic Phase Addition of Anionic/Non-
587 Ionic Surfactants to Poly(Paraphenyleneterephthalamide) Thin Film Composite Nanofiltration
588 Membranes. *Chem. Eng. Process. Process Intensif.* **2016**, *106*, 13–25.
589 <https://doi.org/10.1016/j.cep.2015.11.016>.

590 (38) Jiang, C.; Tian, L.; Zhai, Z.; Shen, Y.; Dong, W.; He, M.; Hou, Y.; Niu, Q. J. Thin-Film Composite
591 Membranes with Aqueous Template-Induced Surface Nanostructures for Enhanced
592 Nanofiltration. *J. Memb. Sci.* **2019**, *589* (July), 117244.
593 <https://doi.org/10.1016/j.memsci.2019.117244>.

594 (39) Schott, H. Hydrophilic–Lipophilic Balance, Solubility Parameter, and Oil–Water Partition
595 Coefficient as Universal Parameters of Nonionic Surfactants. *J. Pharm. Sci.* **1995**, *84* (10), 1215–
596 1222. <https://doi.org/10.1002/jps.2600841014>.

597 (40) Dinarvand, R.; Moghadam, S. H.; Sheikhi, A.; Atyabi, F. Effect of Surfactant HLB and Different
598 Formulation Variables on the Properties of Poly-D,L-Lactide Microspheres of Naltrexone
599 Prepared by Double Emulsion Technique. *J. Microencapsul.* **2005**, *22* (2), 139–151.

600 https://doi.org/10.1080/02652040400026392.

601 (41) Boyd, J.; Parkinson, C.; Sherman, P. Factors Affecting Emulsion Stability, and the HLB Concept. *J.*
602 *Colloid Interface Sci.* **1972**, *41* (2), 359–370. https://doi.org/10.1016/0021-9797(72)90122-1.

603 (42) Chen, G. E.; Liu, Y. J.; Xu, Z. L.; Tang, Y. J.; Huang, H. H.; Sun, L. Fabrication and Characterization of
604 a Novel Nanofiltration Membrane by the Interfacial Polymerization of 1,4-Diaminocyclohexane
605 (DCH) and Trimesoyl Chloride (TMC). *RSC Adv.* **2015**, *5* (51), 40742–40752.
606 https://doi.org/10.1039/c5ra02560e.

607 (43) Branzoi, F.; Branzoi, V. Investigation of Some Nonionic Surfactants as Corrosion Inhibitors for
608 Carbon Steel in Sulfuric Acid Medium. *Int. J. Electrochem. Sci.* **2017**, *12* (8), 7638–7658.
609 https://doi.org/10.20964/2017.08.27.

610 (44) Ren, W.; Tian, G.; Jian, S.; Gu, Z.; Zhou, L.; Yan, L.; Jin, S.; Yin, W.; Zhao, Y. TWEEN Coated NaYF
611 4:Yb,Er/NaYF 4 Core/Shell Upconversion Nanoparticles for Bioimaging and Drug Delivery. *RSC*
612 *Adv.* **2012**, *2* (18), 7037–7041. https://doi.org/10.1039/c2ra20855e.

613 (45) Wenzel, R. N. Surface Roughness and Contact Angle. *J. Phys. Chem.* **1949**, *53* (9), 1466–1467.

614 (46) Onaizi, S. A. Dynamic Surface Tension and Adsorption Mechanism of Surfactin Biosurfactant at
615 the Air–Water Interface. *Eur. Biophys. J.* **2018**, *47* (6), 631–640. https://doi.org/10.1007/s00249-
616 018-1289-z.

617